ACS OMEGA

http://pubs.acs.org/journal/acsodf

Article

N,Cl-Codoped Carbon Dots from *Impatiens balsamina* L. Stems and a Deep Eutectic Solvent and Their Applications for Gram-Positive Bacteria Identification, Antibacterial Activity, Cell Imaging, and ClO^- Sensing

Shaochi Liu, Tian Quan, Lijuan Yang, Linlin Deng, Xun Kang, Manjie Gao, Zhining Xia,* Xiang Li,* and Die Gao*

Cite This: *ACS Omega* 2021, 6, 29022−29036

Read Online

ACCESS | Metrics & More | Article Recommendations | Supporting Information

ABSTRACT: In this study, we first synthesized metal-free N,Cl-doped carbon dots (N,Cl-CDs) using *Impatiens balsamina* L. stems as green precursors in a deep eutectic solvent (DES). The obtained N,Cl-CDs were characterized through transmission electron microscopy (TEM), X-ray photoelectron spectroscopy (XPS), X-ray diffraction (XRD), Fourier-transform infrared (FT-IR) spectroscopy, fluorescence (FL) spectroscopy, and ultraviolet (UV) spectroscopy. In addition to the common features of carbon dots (CDs), such as high light stability, small size, low toxicity, good aqueous solubility, and favorable biocompatibility, these N,Cl-CDs exhibited excellent recognition and selectivity for Gram-positive bacteria by doping with N and Cl elements using DES. The N,Cl-CDs with positive charge cannot only differentiate Gram-positive bacteria by selective fluorescence imaging but also have antibacterial effects on Gram-positive bacteria. Through potential, ROS, and morphological analyses of bacteria before and after treatment with N,Cl-CDs, the antibacterial mechanisms of bacteriostasis, *Enterococcus faecium*, *Staphylococcus aureus*, *Bacillus subtilis*, *Escherichia coli*, *Pseudomonas aeruginosa*, and *Salmonella* were explored. In addition, N,Cl-CDs demonstrated low cytotoxicity and good cell imaging ability in cancer and normal cells. Moreover, they can be used as a fluorescence sensor for the detection of ClO^- with a detection range from 100 nM to 40 μM and a limit of detection (LOD) of 30 nM. In summary, the prepared N,Cl-CDs could be applied as environmentally friendly Gram-positive bacterial identification and antibacterial agents. Additionally, their cell imaging and ClO^- detection abilities were outstanding.

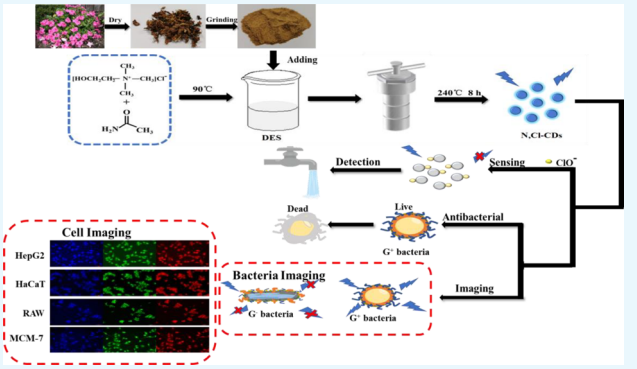

1. INTRODUCTION

Bacterial infection in areas such as food, medical, and environmental fields is a global challenge to human health since it is one of the leading causes of death globally.[1] Although antibiotic therapy is the most widely used and relatively effective treatment method for infection, the gradual emergence of antibiotic resistance has increased the number of bacterial infections.[2,3] Thus, it is crucial to develop alternative and potent antibacterial agents, for which bacteria have not yet developed a resistance, for the clinical treatment of bacterial infection. In addition, it is of great important to distinguish Gram bacteria before antibiotic treatment. Not only identification can preliminarily identify bacteria, but also the Gram bacteria have different mechanisms of action and show different sensitivities to different antibiotics. So, identification of pathogenic bacteria can provide a basis for treatment.

Carbon dots (CDs) are a type of innovative fluorescent NP because of their unique properties such as outstanding optical properties, low cytotoxicity, and good biocompatibility.[4] This outstanding functional material has been widely applied in sensing,[5] biological imaging and therapeutics,[6] drug delivery,[7] and photocatalysis.[8] Moreover, owing to their adjustable size and surface charge characteristics, light-induced redox processes, and membrane disruption ability in the antibacterial process, CDs could be used as antibacterial agents. In recent years, with the requirement of green and sustainable development, more and more researchers give attention to the use of green raw materials to prepare needed materials such as CDs.[9] Thus, the use of natural biomass with an antibacterial effect as

Received: July 30, 2021
Accepted: October 8, 2021
Published: October 21, 2021

green precursors for the development of CDs, which exhibit antimicrobial activity, has attracted significant attention.

Several studies have shown that using natural biomass with antibacterial activity as precursors could effectively obtain CDs with the same activity.[10−14] Boobalan et al. successfully used mushroom as a precursor to prepare CDs and the CDs demonstrated the efficient antibacterial activity against three bacterial strains.[12] Shahshahanipour and co-workers synthesized CDs by a *Lawsonia inermis* (Henna) plant without adding any chemical reagent and they found that CDs had antibacterial activities against Gram-positive and Gram-negative bacteria.[13] However, these CDs only have antimicrobial activity and cannot be used to fast identify unknown bacteria. Until now, although a few studies reported several kinds of CDs that can simultaneously kill and identify bacteria,[15−18] they have some disadvantages: (1) Most of them synthesize CDs using chemical components such as glycerol and dimethyloctadecyl[3-(trimethoxysilyl) propy]ammonium chloride[17] as precursors. (2) Some of their antimicrobial activity comes not from the CDs themselves but from the materials such as genipin[18] and lauryl betaine[15] modified on the CDs. (3) The QYs of the modified CDs will decrease, which is not conducive to the imaging of bacteria or other fluorescence applications. Therefore, it is very necessary to prepare high-QY CDs with both antibacterial and bacterial identification effects using natural biomass as precursors.

Impatiens balsamina L. stems, named "Fengxianhua" in Chinese, are a type of Chinese herbal medicine with antioxidant, antibacterial, and anti-allergic properties.[19] Moreover, *I. balsamina* L. stems not only have a high medicinal value but also have a great application value in the field of food. It is reported that the high contents of natural antioxidants, including rutin, quercetin, and kaempferol, in *I. balsamina* L. stems let them become a new type of food additive.[20] In addition, *I. balsamina* L. stems also are a unique food and can be used to prepare healthy drinks. Various ingredients such as phenolic acids, flavonoids, and naphthoquinones[20] have made *I. balsamina* L. stems a good candidate for preparing CDs with antibacterial and bacterial identification effects. However, until now, *I. balsamina* L. stems have not been studied as precursors for preparing antibacterial CDs. Therefore, it is of academic interest to explore its potential use.

Nevertheless, using water as a solvent to prepare CDs could not significantly improve the QY of CDs, which would affect the potential of CDs for fluorescence identification of bacteria. Recently, several studies have already established that heteroatom doping of nitrogen, sulfur, boron, fluorine, and chlorine in the structure of CDs is an effective method for improving the photoluminescence, antioxidant, and pro-oxidant properties as well as antibacterial activity of CDs.[21−24] Nevertheless, these green precursors contain various ingredients, and most of the CDs prepared using them have doped a small number of heteroatoms (specifically nitrogen) in their structure.[25,26] To further improve the antibacterial activity and bacterial identification ability of the developed CDs, the amount of heteroatom doping in CDs needs to be increased. There are two methods for improving the number of heteroatoms: (1) using precursors that contain these elements and (2) the reaction solvent should contain these elements and it should be employed in the formation of CDs. The former method is not suitable for our research. Therefore, solvents that are environmentally friendly and effective alternatives to water should be developed.

Deep eutectic solvents (DESs) have attracted our attention because of their low cost, nontoxicity, wide dissolution range, and good biocompatibility.[27] DESs are ideal solvents and doping agents for synthesizing doped CDs because they contain abundant elements.[28,29] In our previous studies, DESs were first successfully used as solvents and doping agents for designing N-doped CDs using *Sophora flavescens* Aiton as green precursors. The obtained CDs exhibited high quantum yield (QY), outstanding fluorescence, and detection performance.[30] Thus, in this study, DESs were applied as solvents and doping agents to prepare CDs.

Herein, to synthesize N,Cl-doped CDs (N,Cl-CDs) with fast identification of the Gram-positive and Gram-negative bacteria and antibacterial activity, *I. balsamina* L. stems and DES [ChCl as a hydrogen-bonding acceptor (HBA) and acetamide as a hydrogen-bonding donor (HBD)] were applied as a green precursor and solvent as well as doping agent, respectively. The N,Cl-CDs demonstrated outstanding fluorescence properties and could selectively identify and image Gram-positive bacteria. Simultaneously, they could kill these Gram-positive bacteria by producing free radicals. In addition, considering the advantages of CDs in fluorescence detection and cell imaging, we explored the potential of the developed CDs for ion detection and cell imaging to utilize the developed CDs fully. The obtained N,Cl-CDs can be used effectively in cell imaging and selective detection of ClO^- with a limit of detection (LOD) of 30 nM. To the best of our knowledge, this is the first report of the development of N,Cl-CDs using natural biomass as green precursors with DES as a solvent, and the N,Cl-CDs exhibited multiple functions for bacterial identification, antibacterial activity, ClO^- sensing, and bio-imaging.

2. EXPERIMENTAL SECTION

2.1. Preparation of DESs. The preparation process of DESs was based on a latest report.[31] For details, they can be seen in the Supporting Information.

2.2. Preparation of N,Cl-CDs in DESs. Hydrothermal method was used to prepare the N,Cl-CDs. Two grams of *I. balsamina* L. stem powder was added to 20 mL of DES (DES was composed of chlorine chloride and acetamide at a molar ratio of 1:1), and ultrasonication was performed for 30 min. A brown liquid was obtained and transferred into a 50 mL Teflon-equipped stainless-steel autoclave, which was heated at 240 °C for 8 h. Thereafter, the autoclave was cooled to room temperature and the products were centrifuged at 10,000 rpm for 10 min. To improve the purification of the N,Cl-CDs, the solution was dialyzed in ultrapure water for 24 h using a dialysis bag (retained molecular weight of 1000 Da), and the product was filtered through a 0.22 μm membrane filter. Before further application, the obtained brown solution of N,Cl-CDs was concentrated via evaporation and then freeze-dried. The QY of the N,Cl-CDs was acquired using a slope method with quinine sulfate dissolved in 0.1 M H_2SO_4 (QY = 54%) as the standard fluorophore. The details can be found in the Supporting Information.

2.3. Fluorescence Identification and Imaging of Gram-Positive Bacteria. Six species of bacteria including three types of Gram-negative bacteria [*Escherichia coli* (*E. coli*), *Pseudomonas aeruginosa* (*P. aeruginosa*), and *Salmonella*] and three types of Gram-positive bacteria [*Staphylococcus aureus* (*S. aureus*), *Enterococcus faecium* (*E. faecium*), and *Bacillus subtilis* (*B. subtilis*)] were selected to evaluate the selective fluorescence identification and imaging ability of the N,Cl-CDs. These

https://doi.org/10.1021/acsomega.1c04078
ACS Omega 2021, 6, 29022−29036

Scheme 1. Preparation Process and Applications of N,Cl-CDs

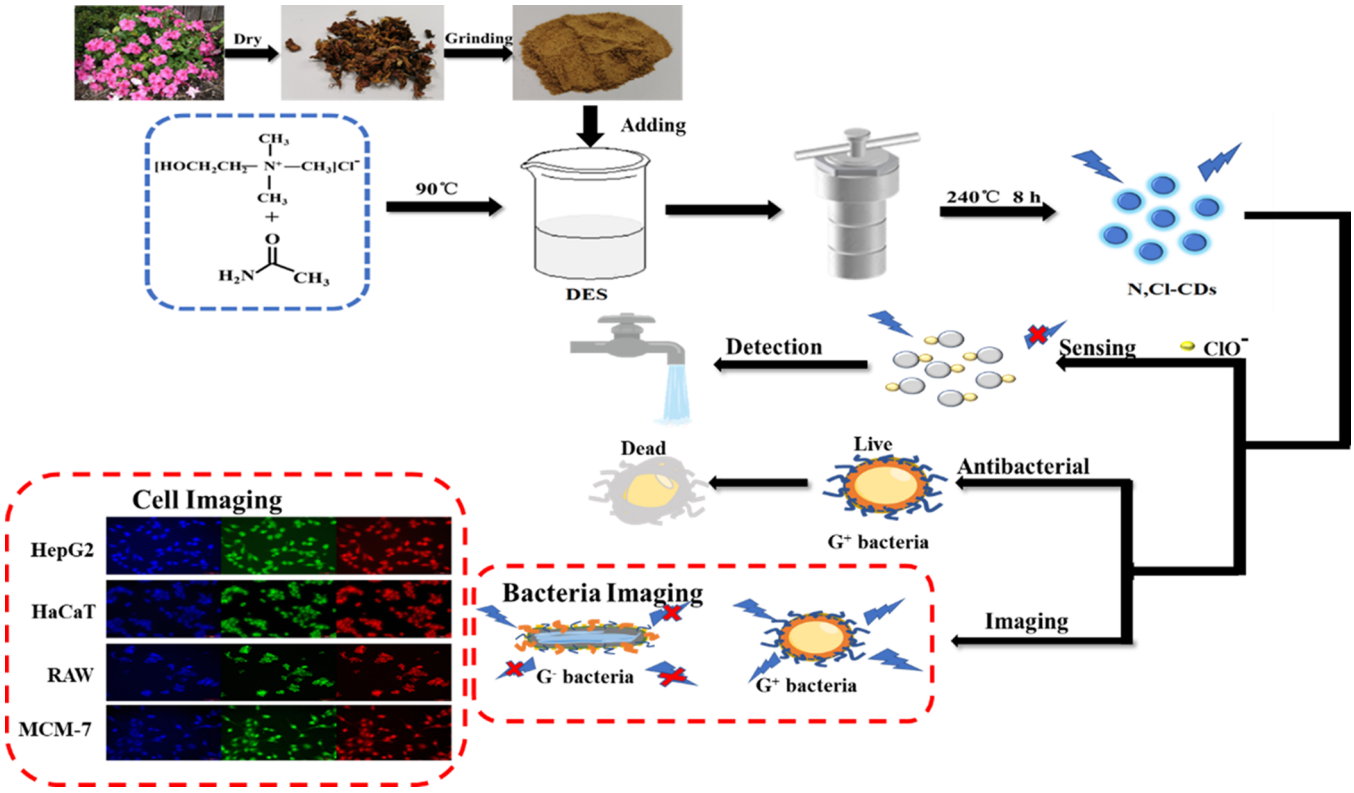

bacterial cells were incubated in trypticase soy broth (TSB) medium and cultured in a vibrating incubator for 12 h at 37 °C. Thereafter, the bacterial cells were exposed to N,Cl-CDs at a concentration of 500 $\mu g \cdot mL^{-1}$ and cultured for 2 h at 37 °C. Subsequently, they were washed three times with PBS to remove excess N,Cl-CDs and observed under a fluorescence inverted microscope further.

2.4. Antibacterial Activity of N,Cl-CDs and the Analysis of ROS. Six species of bacteria were cultured to study their antibacterial activity of the N,Cl-CD on them. To purify the bacteria, a single colony was picked from the TSB agar plate and incubated in TSB liquid medium at 37 °C for 10−16 h. The bacteria were treated separately with different concentrations of N,Cl-CDs in the early exponential phase in a 96-well plate, and then the mixture was incubated under the same light conditions at 37 °C for 24 h. Before monitoring the bacterial growth by testing the optical densities at 600 nm (OD_{600}), the 96-well plates were shaken to mix the liquid. The minimum inhibitory concentration (MIC) value of the N,Cl-CDs was denoted by the observed absence of growth. Therefore, the inoculating loop was dipped in the liquid in the 96-well plate, and the mixture was distributed homogeneously on TSB agar plates. TSB agar plates were observed after culturing at 37 °C for 24 h.

For ROS detection experiments, the Gram-positive bacteria were cultured as described above. DCFH-DA is a common oxidation-sensitive fluorescent probe for determining intracellular ROS.[32] Herein, the DCFH-DA-based method was applied to the analysis of ROS. Briefly, bacterial cell suspensions were treated with N,Cl-CDs (2 $mg \cdot mL^{-1}$) for 2 h. Thereafter, the bacterial cells were washed three times with PBS buffer to eliminate N,Cl-CDs, and then fresh medium was added. DCFH-DA was then added to the mixture at a ratio of 1:1000 and cultured for 30 min. Finally, bacteria were washed three times with PBS to remove excess DCFH, and the fluorescence intensity was monitored using a synergy H1 microplate reader.

2.5. Cytotoxicity of N,Cl-CDs and Cell Imaging. *2.5.1. Cytotoxicity of N,Cl-CDs.* HepG2, HaCaT, RAW, and MCM-7 cells were used to test the cytotoxicity of N,Cl-CDs. First, cells were seeded in a 96-well plate and cultured in a 5% CO_2 incubator for 24 h. Thereafter, they were incubated with different concentrations of N,Cl-CDs (0, 0.1, 0.2, 0.4, 0.6, 0.8, 1.0, 2.0, and 3.0 $mg \cdot mL^{-1}$) for 24 h. Afterward, 10 μL of PBS containing MTT (5 $mg \cdot mL^{-1}$) was added to each well. After incubation for 4 h, the medium was removed, and 150 μL of DMSO was added to each well. The optical absorbance was measured at 570 nm.

2.5.2. Cell Imaging. HepG2, HaCaT, RAW, and MCM-7 cells were used as model cells for cell imaging studies. First, cells were seeded into 6-well plates and incubated at 37 °C in a humidified atmosphere containing 5% CO_2 until the cells adhered to the surface of the plate. Thereafter, the culture medium was replaced with 1 mL of PBS buffer (pH 7.4) containing 500 $\mu g \cdot mL^{-1}$ N,Cl-CDs. After incubation for 30 min, the supernatant was removed, and the cells were washed three times with PBS. All images were captured using a fluorescence inverted microscope.

2.6. Application of N,Cl-CDs in Determination of ClO^-. To study the sensitivity of N,Cl-CDs to ClO^-, 300 μL of different concentrations of ClO^- solution was added to a 2.7 mL of N,Cl-CD solution. The fluorescence intensity of the N,Cl-CD solution after reacting with different concentrations of ClO^- was measured at an excitation wavelength of 340 nm. In addition, to evaluate the selectivity of N,Cl-CDs to ClO^- further, the fluorescence quenching effects of different ions (100 μM) on N,Cl-CDs were evaluated in the presence or absence of ClO^-.

https://doi.org/10.1021/acsomega.1c04078
ACS Omega 2021, 6, 29022−29036

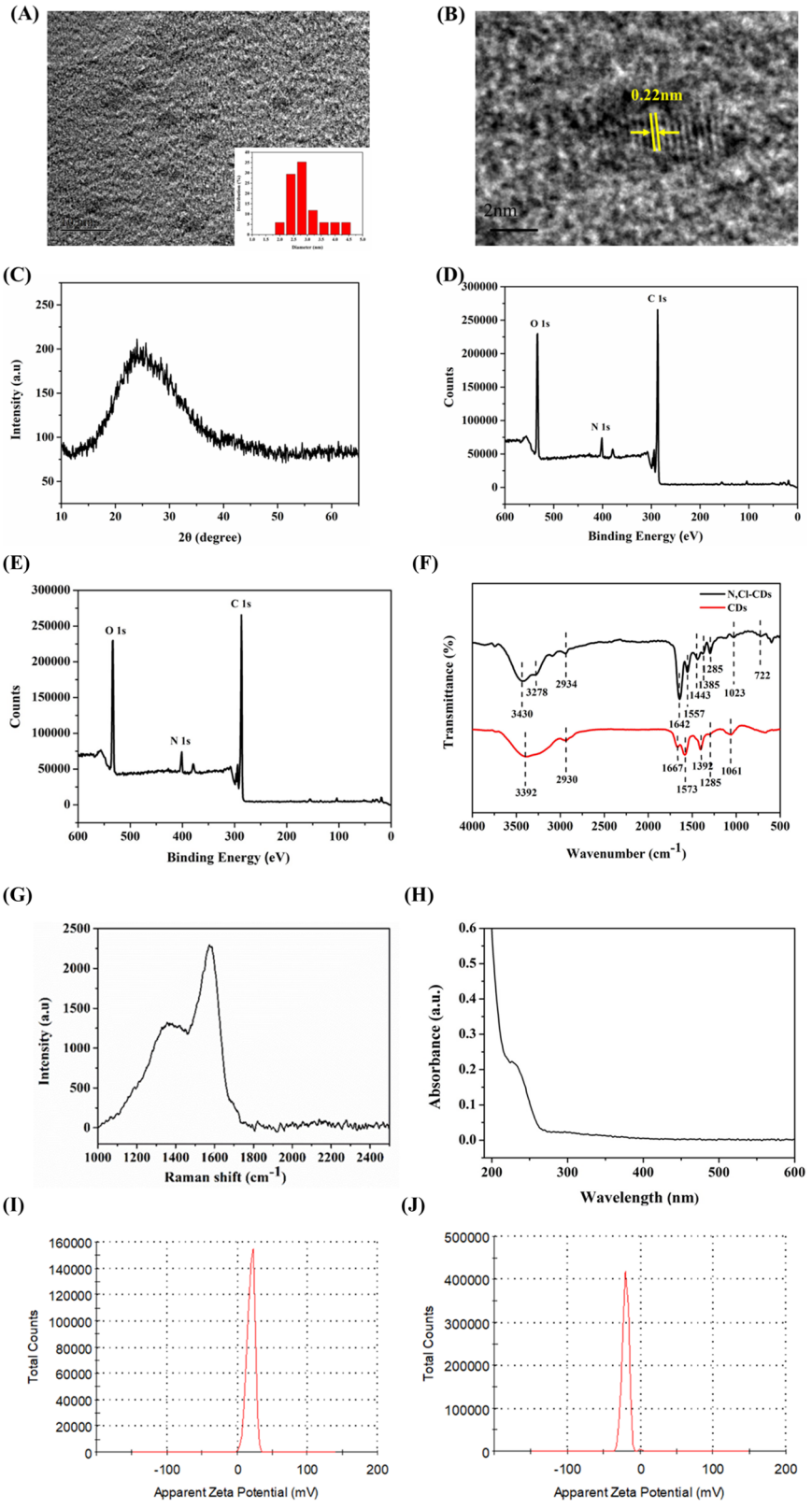

Figure 1. (A) TEM image of N,Cl-CDs (the inset shows the diameter distribution of N,Cl-CDs calculated from the TEM image). (B) HRTEM image of N,Cl-CDs. (C) XRD pattern of N,Cl-CDs. (D) XPS spectra of CDs. (E) XPS spectra of N,Cl-CDs. (F) Raman spectrum of N,Cl-CDs. (G) FT-IR spectra of N,Cl-CDs and CDs. (H) UV−vis absorption of N,Cl-CDs. (I) Apparent zeta potential of N,Cl-CDs. (J) Apparent zeta potential of CDs.

2.7. Determination of ClO^- in Real Water Samples. Local tap water (Luzhou, Sichuan Province) was collected as a real sample and filtered through a 0.22 μm membrane filter to remove impurities. Thereafter, ClO^- was added to obtain different concentrations of tap water (0, 5, 10, and 20 μM). The fluorescence intensity at 420 nm of the mixture was detected using a fluorescence spectrometer, and all experiments were repeated three times under similar conditions.

https://doi.org/10.1021/acsomega.1c04078
ACS Omega 2021, 6, 29022−29036

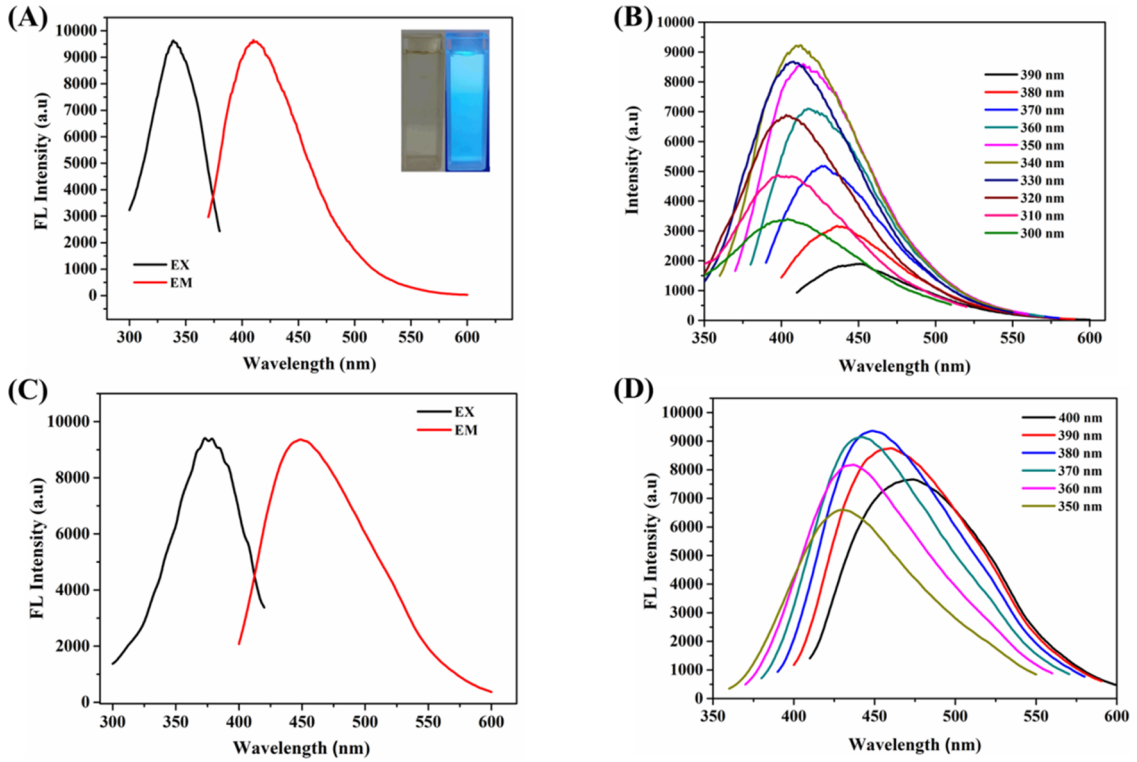

Figure 2. (A) Fluorescence excitation and emission spectra of N,Cl-CDs (insets show the images of N,Cl-CD solution under visible light and UV light of 365 nm). (B) Fluorescence emission spectra of N,Cl-CDs with different excitation wavelengths (from 300 nm to 390 nm). (C) Fluorescence excitation and emission spectra of CDs. (D) Fluorescence emission spectra of CDs with different excitation wavelengths (from 350 nm to 400 nm).

The preparation process and application of N,Cl-CDs are shown in Scheme 1.

3. RESULTS AND DISCUSSION

3.1. Synthesis of N,Cl-CDs. CDs were prepared via a one-step hydrothermal method using *I. balsamina* L. stems and DES as the solvent as well as doping agent. To investigate the effect of different DESs on the QY of CDs, 10 types of DESs were successfully prepared using different HBAs and HBDs (shown in Figure S1A,B), and a definition of the exact composition of DES tested in each case is shown in Table S1. Further, these DESs were applied as a solvent and doping agent for preparing CDs doped with different elements. As summarized in Table S1, CDs (N,Cl-CDs) prepared using DES with ChCl as HBA and acetamide as HBD had the highest QY of 15.64%. Furthermore, the main factors (including the water content of DES, dosage of *I. balsamina* L. stems, reaction temperature, and reaction time) that may influence the QY of CDs were optimized. The optimal reaction conditions were as follows: 20 mL of DES as the solvent with 0% water, 1 g of *I. balsamina* L. stems as precursors, 240 °C as the reaction temperature, and 8 h as the reaction time. The highest QY of N,Cl-CDs obtained was 24.36% (see Table S2 and Figure S2A−C). In comparison with the CDs prepared using water as the solvent (QY was 11.63%), the QY of N,Cl-CDs significantly improved, indicating that heteroatom doping in the CD structure improved the fluorescence properties of the CDs. Compared with the proposed bifunctional CDs, which simultaneously have bacterial detection (by fluorescence) and inhibition, their QY is significantly higher compared to those of the existing material.[15,17,18] Therefore, it is conducive for bacterial detection.

3.2. Characterization of N,Cl-CDs. Various measurements were made to characterize the obtained N,Cl-CDs. TEM images revealed that the N,Cl-CDs had good dispersity and uniformity, and the average size distribution was between 2 and 4.5 nm (Figure 1A). Moreover, the high-resolution TEM (HRTEM) image (Figure 1B) showed that significant fringe spacing existed in the N,Cl-CDs and the crystal lattice spacing was 0.22 nm, which suggests the presence of a typical graphene facet (100) plane.[33] Furthermore, the XRD pattern in Figure 1C exhibited two dominant peaks around $2\theta = 24.1°$ and $2\theta = 40.7°$, which correspond to the (002) and (100) lattice spacing of carbon-based materials existing in the N,Cl-CD structure.[34,35] The TEM data and XRD results provide strong evidence for the successful synthesis of N,Cl-CDs.

To verify that the Cl and N atoms were doped successfully, N,Cl-CDs and CDs (prepared using water as a solvent) were characterized via XPS, FT-IR, UV−vis spectroscopy, and ζ-potential. The elemental contents of the N,Cl-CDs and CDs were first investigated using XPS. As summarized in Table S3, CDs were composed of C, O, and a small amount of N (5.71%), whereas N,Cl-CDs contained C, O, N (15.99%), and Cl (8.29%). The elemental content of N in N,Cl-CDs was approximately three times that in CDs. These results indicated that DES could be a great substitute for conventional N and Cl sources. Furthermore, the differences in the surface functional group between the N,Cl-CDs and CDs were studied through XPS scans of the two types of CDs. As shown in Figure 1D, the results indicated that C 1s, N 1s, and O 1s peaks existed in the CDs at 284.85, 399.61, and 531.88 eV, respectively. The high-resolution C 1s peaks exhibited three peaks at 284.80, 285.94, and 287.90 eV, which were attributed to C−C, C═N, and C═O, respectively (Figure S3A).[36,37] The N 1s spectra showed two

https://doi.org/10.1021/acsomega.1c04078
ACS Omega 2021, 6, 29022−29036

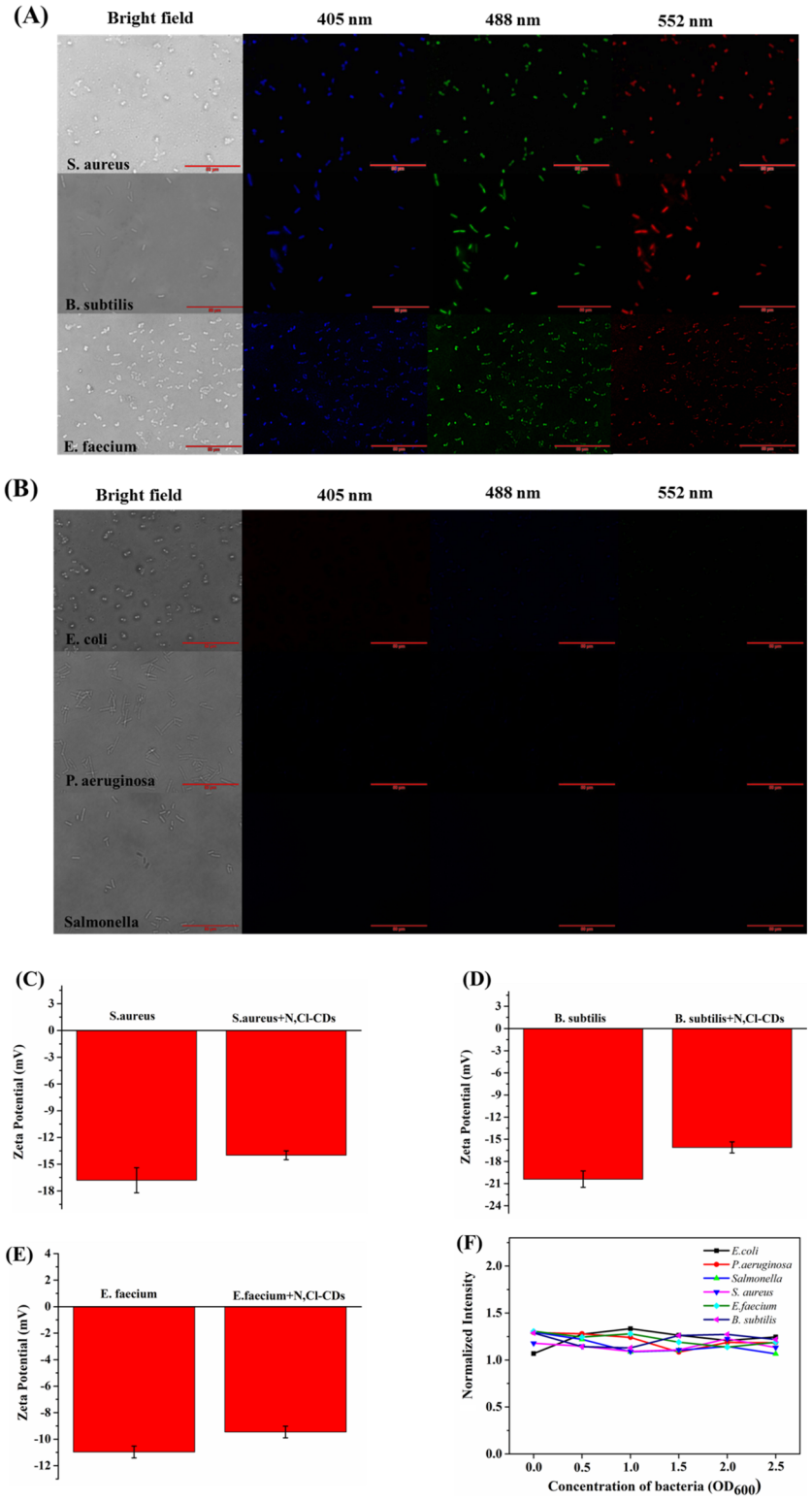

Figure 3. (A) Fluorescence images of *S. aureus*, *B. subtilis*, and *E. faecium* after incubation with N,Cl-CDs under the excitation wavelengths of 405, 488, and 552 nm. (B) Fluorescence images of *E. coli*, *P. aeruginosa*, and *Salmonella* after incubation with N,Cl-CDs under 405, 488, and 552 nm excitation wavelengths. (C) Zeta potential of *S. aureus* and *S. aureus* with N,Cl-CDs. (D) Zeta potential of *B. subtilis* and *B. subtilis* with N,Cl-CDs. (E) Zeta potential of *E. faecium* and *E. faecium* with N,Cl-CDs. (F) Fluorescence intensity of N,Cl-CDs after interaction with different concentrations (OD_{600} = 0−2.5) of bacteria.

peaks: pyrrolic-N and pyridinic-N at 399.60 and 401.70 eV, respectively (Figure S3B).[37] In addition, the spectrum of O 1s can be divided into two peaks including C═O and C−O banded at 531.10 and 532.26 eV, respectively (Figure S3C).[37,38]

In the XPS spectrum of N,Cl-CDs (Figure 1E), four predominant peaks including Cl 2p, C 1s, N 1s, and O 1s peaks were observed at 198.61, 287.13, 401.67, and 532.79 eV, respectively. The Cl 2p spectrum displayed two peaks at 198.60

https://doi.org/10.1021/acsomega.1c04078
ACS Omega 2021, 6, 29022−29036

eV (N−Cl) and 200.18 eV (C−Cl) (Figure S4A).[39,40] The C 1s spectrum exhibited three peaks that were subtly different from those of the CDs. Deconvolution of the C 1s spectrum (Figure S4B) verified the existence of C−O (286.20 eV), C−Cl (287.41 eV), and C═O (289.15 eV).[41−43] In addition, the N 1s XPS spectrum (Figure S4C) exhibited two peaks at 401.30 (C−N) and 403.00 eV (pyridinic-N).[37,44] The O 1s XPS spectrum (Figure S4D) exhibited two peaks at 532.60 and 533.55 eV, which corresponded to C−O and O═C—OH, respectively.[33,45] FT-IR was used to characterize the N,Cl-CDs and CDs further. Figure 1F shows that broad absorption peaks at ∼3390, ∼2930, ∼1650, ∼1560, ∼1390, ∼1285, and ∼1040 cm^{-1}, which were attributed to the O−H, C−H, C═O, C═N, C−N, C−O, and C−C stretching vibrations, respectively, existed in the FT-IR spectra of N,Cl-CDs and CDs. However, compared with CDs, N,Cl-CDs had three characteristic absorption peaks at 3278, 1443, and 722 cm^{-1}, which correspond to N−H stretching vibration, N−H bending vibration, and C−Cl stretching vibration, respectively.[43] This result further proved that Cl and N atoms were doped successfully in N,Cl-CDs. Furthermore, the Raman spectrum of N,Cl-CDs was measured. The Raman spectrum of the N,Cl-CDs in Figure 1G revealed that the majority of N,Cl-CDs produced were predominantly graphitic in nature. The G peak at ∼1590 cm^{-1} and the D peak at ∼1390 cm^{-1} were separately attributed to sp^2-hybridized carbons and sp^3-hybridized carbons.[46,47]

Furthermore, the UV−vis absorption of the N,Cl-CDs was measured. Figure 1H shows a clear absorption peak at approximately 240 nm, which corresponds to the $n-\sigma^*$ transition of C−O and C−N bonds in the N,Cl-CDs. Moreover, there was a weak absorption band at approximately 300 nm, which could be attributed to the $n-\pi^*$ transition of C═N and C═O. These results are consistent with those of other characterizations. Notably, a significant difference between the surface charges of the N,Cl-CDs and CDs was observed. As shown in Figure 1I,J, the ζ-potential of CDs was −19.43 mV, whereas that of N,Cl-CDs shifted from a negative potential to a positive potential (22.47 mV) when DES was substituted with water as the solvent. Because a large number of amino groups were introduced into the surface of the CDs, the surface charge of N,Cl-CDs had a large shift, and the positive charge from the amino groups may favor antimicrobial properties.

Additionally, the fluorescence properties of the N,Cl-CDs were investigated. As shown in Figure 2A, the N,Cl-CDs emitted stable blue fluorescence in solution under ultraviolet light, and the value was determined by changing the excitation wavelength from 300 to 390 nm at intervals of 10 nm (Figure 2B). However, the maximal fluorescence emission of the CDs was 450 nm at an excitation wavelength of 380 nm (Figure 2C,D). The difference between the fluorescence properties of N,Cl-CDs and CDs demonstrates that the doping of DES changed the fluorescence properties of the CDs.

Meanwhile, to expand the scope of application of the N,Cl-CDs, the effects of ionic strength, pH, and temperature on the stability and photostability of N,Cl-CDs were studied. As shown in Figure S5A, the fluorescence intensity of N,Cl-CDs in NaCl solutions with different concentrations slightly changed. Moreover, Figure S5B shows that the fluorescence intensity of N,Cl-CDs was slightly affected in both acidic and alkaline solutions. Moreover, the fluorescence intensity of N,Cl-CDs slightly corresponded to temperature (Figure S5C). As can be seen in Figure S5D, the fluorescence intensity was not impacted during 8 h, indicating that the N,Cl-CDs exhibited excellent photostability. Therefore, N,Cl-CDs have good stability under different conditions, and they could be applied in different environments.

3.3. Fluorescence Imaging of Gram-Positive Bacteria. Based on the antibacterial activity of the precursors and the outstanding fluorescence properties of N,Cl-CDs, the fluorescence imaging effects of N,Cl-CDs on six colonies of different bacteria (three Gram-positive and three Gram-negative bacteria) were explored. As shown in Figure 3A,B, three types of Gram-positive bacteria exhibited multicolor fluorescence under different excitation wavelengths through a fluorescence inverted microscope. In contrast, all the three Gram-negative bacteria exhibited no significant fluorescence signals under similar conditions. These results indicate that N,Cl-CDs can be used to identify the Gram-positive bacteria selectively via fluorescence imaging. This could be owing to differences in the heterogeneities of the bacterial surface and bioelectrical environment. It has been reported that the bioelectrical environment of the Gram-positive bacteria is significantly more negatively charged than that of the Gram-negative bacteria.[48] Moreover, the result of the ζ-potential indicates that N,Cl-CDs have a positive charge. Therefore, there is an attractive force (positive and negative charges) between the Gram-positive bacteria and N,Cl-CDs, resulting in an allowance for more N,Cl-CD attachment to the Gram-positive bacteria. To confirm this attachment effect, the ζ-potentials of the mixtures of N,Cl-CDs and Gram-positive bacteria were investigated. It was established that the charge of bacteria was more positive after incubation with N,Cl-CDs (*E. faecium* from −10.97 to −9.46 mV, *S. aureus* from −16.8 to −14.0 mV, and *B. subtilis* from −20.4 to −16.1 mV), indicating that the N,Cl-CDs settled on the surface of bacteria (Figure 3C−E). However, the ζ-potentials of the mixtures of N,Cl-CDs and Gram-negative bacteria had no significant changes (*P. aeruginosa* from −4.29 to −4.26 mV, *E. coli* from −7.71 to −7.66 mV, and *Salmonella* from −3.10 to −2.88 mV), indicating that the N,Cl-CDs settled on the surface of bacteria (Figure S6A−C). The results further demonstrated that the interaction effects of N,Cl-CDs and Gram-negative bacteria were weak.

Moreover, the selectivity could be attributed to the difference in the structure and composition of the cell wall in the Gram-positive and Gram-negative bacteria. It has been reported that the cell wall composition of the Gram-positive bacteria is relatively simple compared to that of the Gram-negative bacteria. Only one membrane and a thicker layer of peptidoglycan containing negatively charged teichoic acids exist in the cell walls of Gram-positive bacteria. The negatively charged teichoic acid on the peptidoglycan layer allows Gram-positive bacteria to have many anionic sites to interact with positively charged N,Cl-CDs.[15] Therefore, under the dual action of the negatively charged bioelectric environment and the characteristics of cell walls, Gram-positive bacteria can easily interact with positive N,Cl-CDs, leading to an increase in the likelihood of damage to the cell wall and thus allowing the N,Cl-CDs to accumulate in the bacteria. Although the peptidoglycan layer of the Gram-negative bacteria is significantly thinner than that of the Gram-positive bacteria, the peptidoglycan layer of the Gram-negative bacteria has an extra outer membrane, which is composed of lipopolysaccharide. Because of the existence of the lipopolysaccharide layer, which is cross-bridged by divalent cations, the outer membrane of the Gram-negative bacteria is not easily penetrated by the N,Cl-CDs.[15] Thus, N,Cl-CDs

https://doi.org/10.1021/acsomega.1c04078
ACS Omega 2021, 6, 29022−29036

cannot have a fluorescence identification effect on the Gram-negative bacteria because of their weak electronegativity and special structural characteristics.

In addition, with reference to other reports, some CDs have imaging-guided bacterial differentiation for the fluorescence intensities of CD increase when the polar environment changed.[17] To verify the mechanism of selective fluorescence imaging of the Gram-positive bacteria, fixed concentrations of N,Cl-CDs were mixed with different concentrations of bacteria and the fluorescence intensities at 420 nm were observed after incubation for 30 min. As shown in Figure 3F, bacteria had no impact on the fluorescence intensity with an increase in the concentration of bacteria. The experiment confirmed that this was not because of the mechanism. The good selectivity for the Gram-positive bacterial cells was because of the positively charged N,Cl-CDs.

3.4. Antibacterial Ability and Antibacterial Mechanism of the N,Cl-CDs. To evaluate the antibacterial activity of N,Cl-CDs further and investigate whether the antibacterial activity of the CDs was significantly improved after doping with N and Cl, the MIC was used to evaluate the antibacterial abilities of N,Cl-CDs and CDs (water as a solvent) against the Gram-positive and Gram-negative bacteria.[49] The bacterial cells were treated with different doses of N,Cl-CDs and CDs, and the OD values of the mixtures were observed using an H1 microplate reader at 600 nm. As shown in Table 1 and Figure 4A−D, the

Table 1. MIC Values of N,Cl-CDs and CDs for Six Species of Bacteria

species	game type	N,Cl-CDs ($mg{\cdot}mL^{-1}$)	CDs ($mg{\cdot}mL^{-1}$)
S. aureus	G+	0.08	2
E. faecium	G+	0.2	1.2
B. subtilis	G+	0.16	2.4
Salmonella	G−	>4	>4
E. coli	G−	>4	>4
P. aeruginosa	G−	>4	>4

inhibitory effects on the Gram-positive bacteria were gradually enhanced with increasing concentration of N,Cl-CDs. The lowest MIC values for *S. aureus*, *E. faecium*, and *B. subtilis* were 0.08, 0.2, and 0.16 $mg{\cdot}mL^{-1}$, respectively. Although CDs also had a certain antibacterial ability, the MIC values against the three Gram-positive bacteria were all greater than 1.2 $mg{\cdot}mL^{-1}$. These results indicated that doping with heteroatoms enhanced the antibacterial ability of N,Cl-CDs.

Notably, N,Cl-CDs and CDs exhibited no antibacterial activity against the Gram-negative bacteria (MIC > 4 $mg{\cdot}mL^{-1}$). This result was consistent with the results of the bacterial fluorescence imaging. Similar to selective fluorescence imaging, the surface compositions of N,Cl-CDs (the surface of the N,Cl-CDs had more passivation terminal groups of $-NH_2$, which was more favored in interacting with negatively charged bacterial cells)[50] and bacteria were the main causes of selective antibacterial properties.[51,52]

To confirm the above conjecture of the effects of N,Cl-CDs on the Gram-positive bacterial cells further, the morphological changes of the Gram-positive bacteria with and without the treatment of N,Cl-CDs were obtained via SEM. The morphology of bacteria in Figure 5A−C shows that there were significant differences before and after stimulation by N,Cl-CDs. The surface of the untreated bacterial cell membranes was integrated, whereas disintegration of the cell membrane was observed after treatment with N,Cl-CDs. Therefore, this effect may be one of the mechanisms of the antibacterial action.

In addition, according to reports in the literature, CDs have some antibacterial effects owing to the production of ROS.[53] The endogenous ROS generation induced by the positively charged CDs was higher than that induced by the negatively charged CDs, and neutral CDs did not induce ROS generation.[54] Hence, N,Cl-CDs could obtain antibacterial effects through the production of ROS, and further research on the endogenous ROS generation area is needed. 2,7-Dichloro fluorescein diacetate (DCFH-DA), a fluorescence probe, was used to monitor ROS.[55] In this study, bacteria with DCFH-DA served as controls. Owing to the fluorescence property of the N,Cl-CDs, the Gram-positive bacteria incubated with N,Cl-CDs were also implemented. As shown in Figure 5D−F, the endogenous ROS of bacterial cells exposed to N,Cl-CDs increased significantly when the fluorescence interference of the N,Cl-CDs was eliminated. This phenomenon demonstrated that another antibacterial mechanism of N,Cl-CDs was through the production of ROS.

3.5. In Vitro Cytotoxicity and Cell Imaging of N,Cl-CDs. To evaluate the potential practical applications of N,Cl-CDs in biosystems further, the biocompatibility and cytotoxic effect of the N,Cl-CDs were tested using an MTT assay. To demonstrate the wide application of this material, two types of cancer cells and two types of normal cells were used. As shown in Figure S7A−D, there was a slight decrease in cell activity after the cells were incubated in N,Cl-CD solution at different concentrations (0 to 3 $mg{\cdot}mL^{-1}$) for 24 h. These results indicated the low toxicity and favorable biocompatibility of the N,Cl-CDs.

Furthermore, N,Cl-CDs were used for the cell imaging. Figure 6A−D shows the tagged cells that were imaged under different excitations, and the cells were illuminated with blue, green, and red lights. From the images, it can be further observed that the N,Cl-CDs did not induce changes in the morphology of cells, indicating that the cell imaging demonstrated that N,Cl-CDs possessed low cytotoxicity to living cells. Thus, N,Cl-CDs have great potential in bio-imaging applications.

3.6. ClO^- Detection by N,Cl-CDs. Considering the advantages of CDs in fluorescence detection, the potential of the developed N,Cl-CDs for fluorescence detection has also been explored. As shown in Figure 7A, in comparison with other ions and substances, including Hg^{2+}, Ca^{2+}, Al^{3+}, K^+, Na^+, Cu^{2+}, Ni^+, Mn^{2+}, Co^{2+}, Br^-, Cl^-, SO_4^{2-}, NO_3^-, HCO_3^-, and H_2O_2, the fluorescence of N,Cl-CDs can be significantly quenched by ClO^-, indicating that N,Cl-CDs can be used as fluorescence sensors for ClO^- detection. The effect of reaction time was tested before investigating the sensitivity of N,Cl-CDs. The signal response of the N,Cl-CDs by ClO^- remained constant after 30 s of adding ClO^- (Figure 7B). Thus, 30 s was the reaction time. Under optimum conditions, the sensitivity of N,Cl-CDs to ClO^- was determined. As shown in Figure 7C,D, the fluorescence intensity showed a good linear relationship with the concentration of ClO^- from 100 nM to 40 μM (R^2 = 0.9903). The equation of linear regression was $F_0/F = 0.01855C + 1.01071$ (C is the concentration of ClO^-, μM) with an LOD of 30 nM based on the formula of 3σ/slope. The results in Table S4 summarize the linear range and LOD of other carbon materials in previous studies. Thus, the effect of N,Cl-CDs was not poor.

To compare the difference between the N,Cl-CDs and CDs for the selective detection of ClO^-, the sensitivity of CDs to ClO^- was studied. Although the fluorescence quenching effect remains after adding the ClO^- solution, the sensitivity of ClO^- is

https://doi.org/10.1021/acsomega.1c04078
ACS Omega 2021, 6, 29022−29036

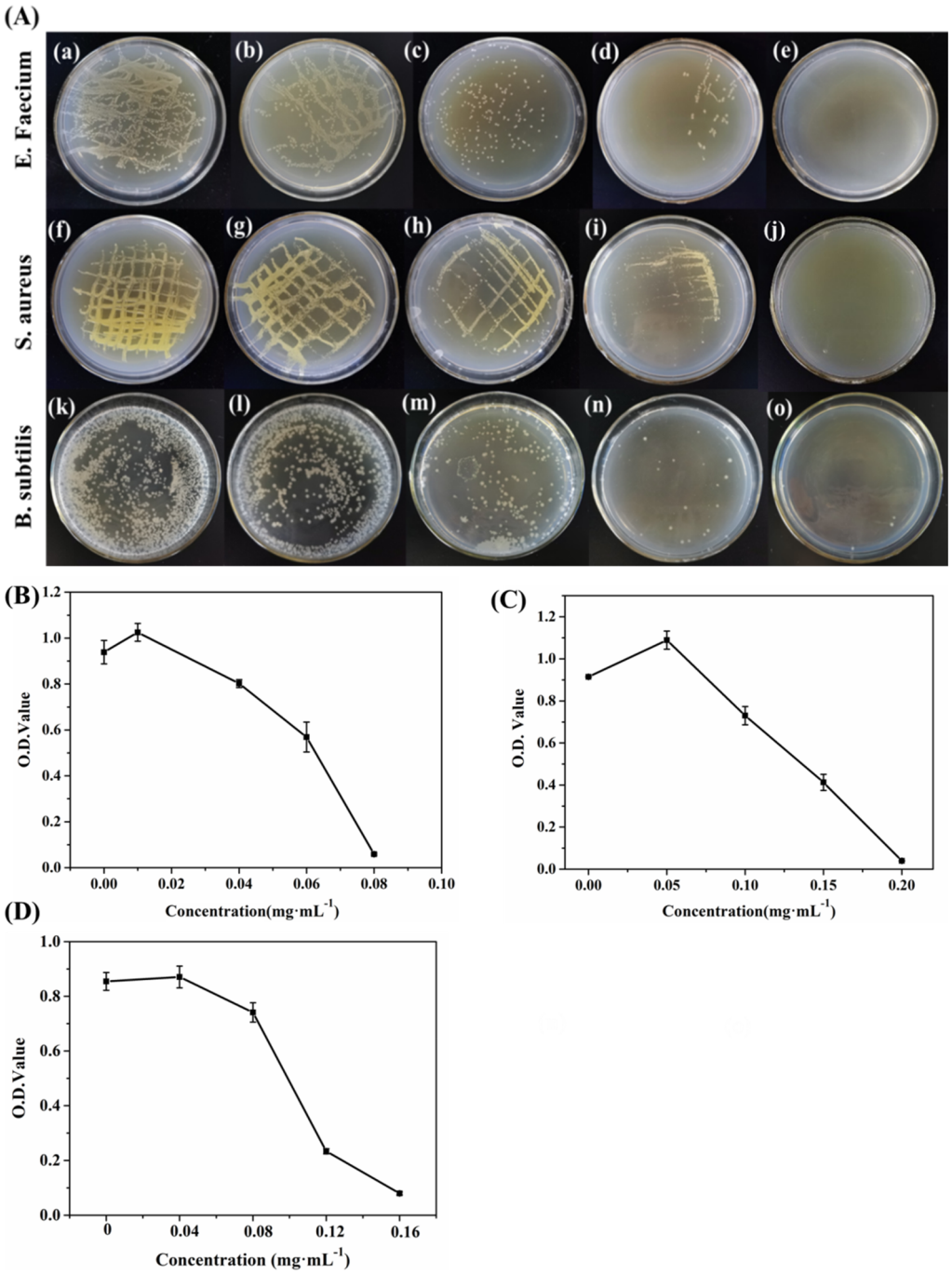

Figure 4. (A) Colony status images of different Gram-positive bacteria after incubation with different doses of N,Cl-CDs. (B) MIC curves of N,Cl-CDs to *S. aureus*. (C) MIC curves of N,Cl-CDs to *B. subtilis*. (D) MIC curves of N,Cl-CDs to *E. faecium*.

lower, indicating that codoping of CDs could improve the optical properties (Figure S8A). Although N,Cl-CDs and CDs exhibited blue fluorescence, N,Cl-CDs exhibited a larger Stokes shift than the CDs. This may lead to the high fluorescence efficiency and anti-interference performance of N,Cl-CDs.[43]

To prove that N,Cl-CDs possess a practical value for low analytical limitation and high sensitivity, tap water from Southwest Medical University was collected to evaluate the performance of the N,Cl-CDs. Because tap water is a complex sample, a standard addition method was used to minimize ionic interference. Before adding ClO^- solutions of a known concentration in water, 6.76 μM ClO^- was established in real water samples using the prepared fluorescence sensor. Furthermore, known concentrations of ClO^- were added to real water sample solutions to evaluate the practicability of the N,Cl-CDs-based fluorescence sensor. The standard addition recoveries of ClO^- ranged from 96.51 to 104.22%, as listed in Table 2. Hence, the developed fluorescence method is nearly free from ionic interference and can meet the detection requirements.

3.7. Mechanism of Fluorescence Detection of ClO^- by N,Cl-CDs. From the latest reports, quenching mechanisms include static quenching, dynamic quenching, Förster resonance energy transfer (FRET), photoinduced electron transfer (PET), and inner filter effect (IFE). To explore the quenching mechanism of N,Cl-CDs to ClO^-, the fluorescence lifetimes

https://doi.org/10.1021/acsomega.1c04078
ACS Omega 2021, 6, 29022−29036

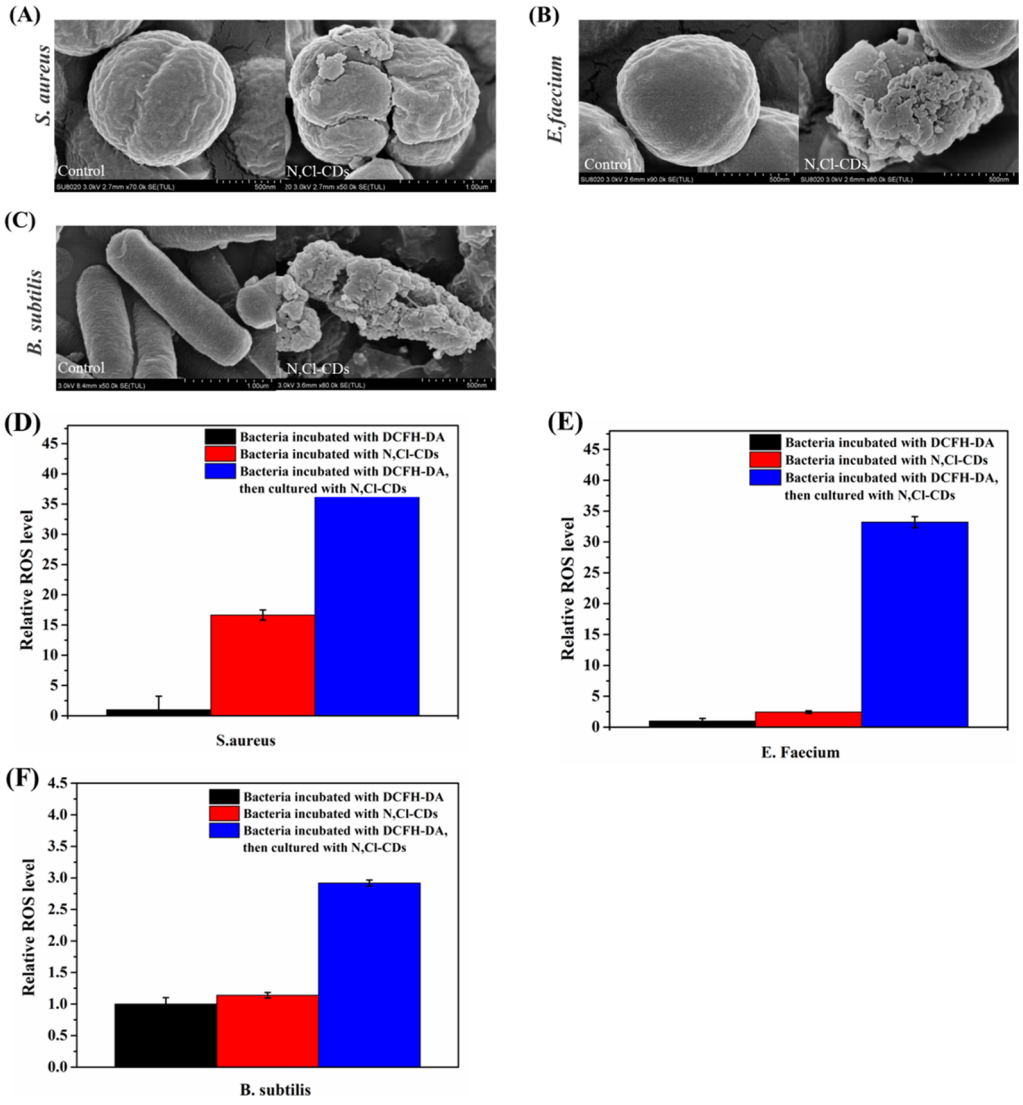

Figure 5. (A) SEM images of *S. aureus* and *S. aureus* after incubation with N,Cl-CDs. (B) SEM images of *B. subtilis* and *B. subtilis* after incubation with N,Cl-CDs. (C) SEM images of *E. faecium* and *E. faecium* after incubation with N,Cl-CDs. (D) Intracellular ROS of *S. aureus* induced by N,Cl-CDs. (E) Intracellular ROS of *B. subtilis* induced by N,Cl-CDs. (F) Intracellular ROS of *E. faecium* induced by N,Cl-CDs.

of N,Cl-CDs and N,Cl-CDs/ClO^- were determined. As shown in Figure S8B, the fluorescence decay spectra could be fitted with a double exponential curve, and the average fluorescence lifetime of N,Cl-CDs was approximately 3.67 ns. However, that of the N,Cl-CDs/ClO^- was 1.52 ns. This significant decline indicated that the quenching effect probably operated as a mechanism of dynamic quenching, FRET, and PET. Furthermore, the UV−vis spectra were performed separately with or without ClO^-. It can be observed from Figure S8C that the UV−vis spectra did not significantly change, indicating that the quenching mechanisms were not static quenching and IFE, which could be used to observe the new absorption peaks of the ground-state complex. Therefore, the quenching effect could be caused by the dynamic quenching mechanism.[56] Moreover, dynamic quenching significantly varies from static quenching; the quenching effect can be enhanced by increasing the temperature. F_0/F with different concentrations of ClO^- was measured at different temperatures, and the Stern−Volmer equation was used to show the fluorescence quenching as follows:

$$F_0/F = 1 + K_{sv}[c]$$

where F_0 and F are the fluorescence intensities in the absence and presence of ClO^-, [c] is the concentration of the quencher, and K_{sv} is the quenching constant. When K_{sv} increased with increasing reaction temperature, dynamic quenching may occur.[56] The result in Figure 8A indicates that the K_{sv} of N,Cl-CDs gradually increased with an increase in temperature. This result indicated that dynamic quenching may be a mechanism of fluorescence detection of ClO^- by N,Cl-CDs. Moreover, FRET requires a certain degree of overlap between the emission band of the fluorophore and the absorption band of the quencher, which causes the fluorescence to be quenched.[57] As shown in Figure 8B, the ultraviolet absorption band of ClO^- just overlapped with the excitation band of N,Cl-CDs. Hence, there could not be a FRET mechanism. To verify whether PET is a mechanism of fluorescence detection of ClO^- by N,Cl-CDs, the highest occupied orbital (HOMO) and lowest unoccupied orbital (LUMO) energy levels of N,Cl-CDs were investigated by using the density functional theory (DFT) method.[58] As described in Figure 8C, the HOMO and LUMO of N,Cl-CDs were −5.511 and −1.946 eV and the HOMO and LUMO of ClO^- were

https://doi.org/10.1021/acsomega.1c04078
ACS Omega 2021, 6, 29022−29036

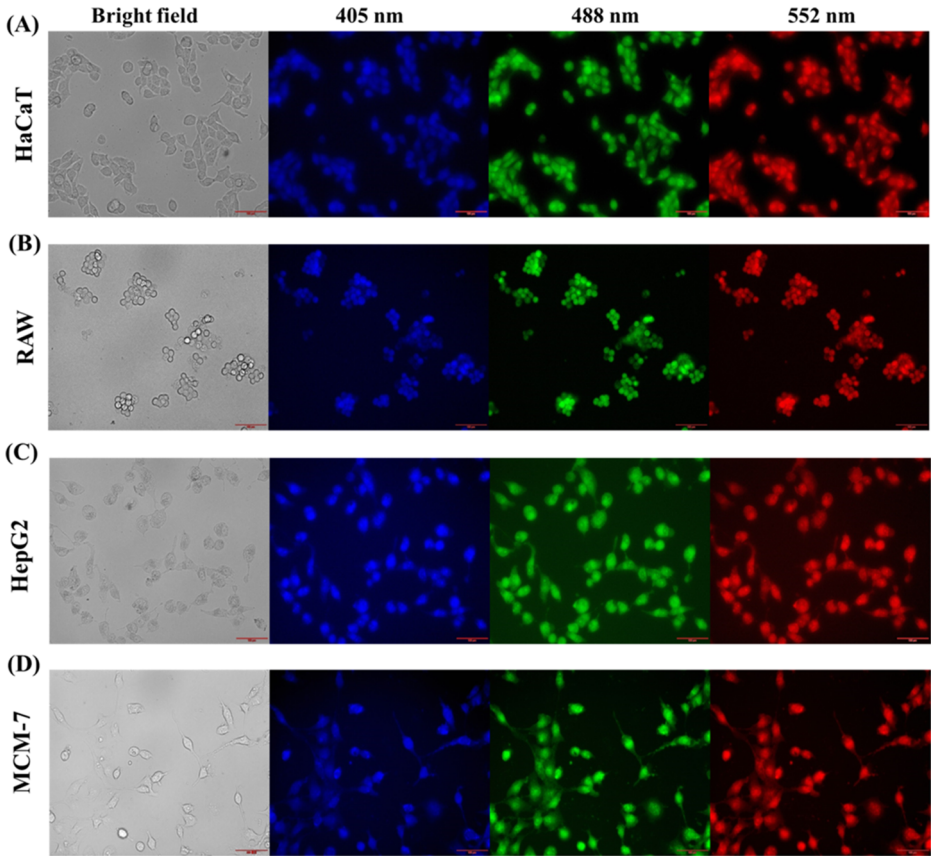

Figure 6. (A) Fluorescence images of HaCaT cells treated with the N,Cl-CDs. (B) Fluorescence images of RAW cells treated with the N,Cl-CDs. (C) Fluorescence images of HepG2 cells treated with the N,Cl-CDs. (D) Fluorescence images of MCM-7 cells treated with the N,Cl-CDs.

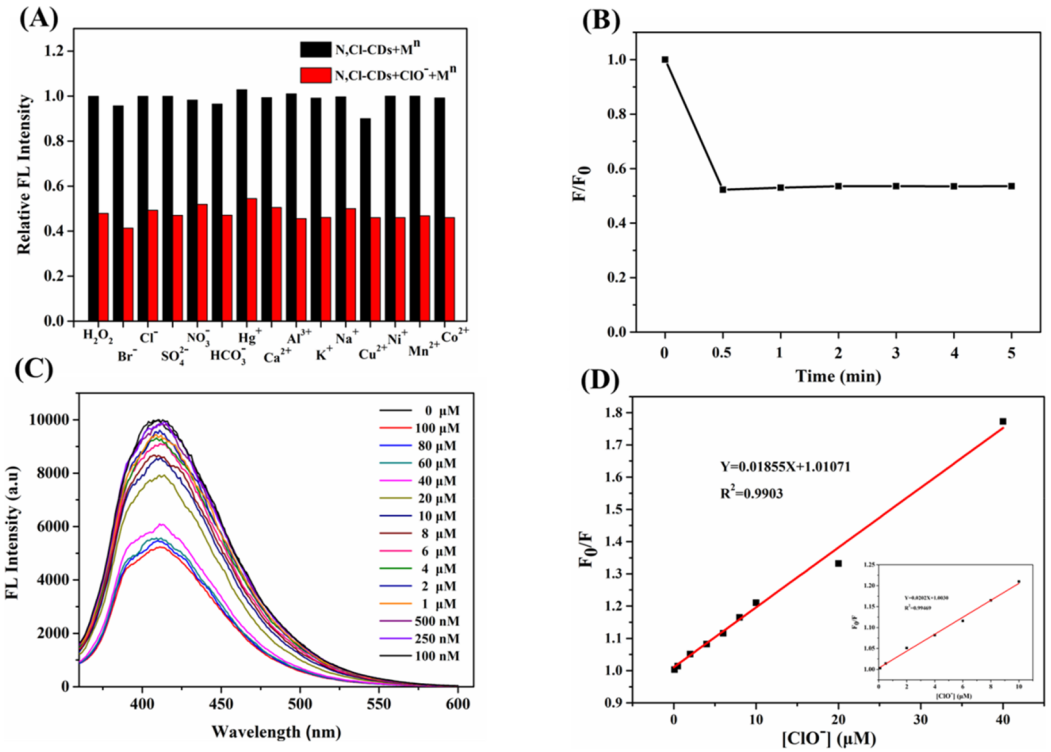

Figure 7. (A) Selectivity of N,Cl-CDs for ClO^- in the presence of other ions. (B) Reaction time of the N,Cl-CDs kept constant after adding ClO^-. (C) Fluorescence emission spectra of N,Cl-CDs in the presence of ClO^- with the concentration of 0−100 μM. (D) Linear curve between F_0/F and the concentration of ClO^- (the inset is a linear curve between F_0/F and the smaller concentration of ClO^-).

https://doi.org/10.1021/acsomega.1c04078
ACS Omega 2021, 6, 29022−29036

Table 2. Recovery of ClO^- in Real Samples

sample	found (μM)	added (μM)	total found (μM)	recovery (%)	RSD (n = 3) (%)
tap water	6.76	20	27.79	104.22	3.70
		10	16.70	99.64	2.45
		5	11.35	96.51	4.04

−3.543 and −6.949 eV, respectively. So, the electron transfer in the excited state of N,Cl-CDs can occur from the LUMO of N,Cl-CDs to the LUMO of ClO^-, indicating that the PET quenching mechanism between N,Cl-CDs and ClO^- was possible.

Therefore, the fluorescence quenching of N,Cl-CDs on ClO^- can be attributed to the dynamic quenching and PET.

4. CONCLUSIONS

In summary, we first synthesized novel N,Cl-CDs using natural biomass *I. balsamina* L. stems as a green precursor and DES as a solvent as well as doping agent. Moreover, as a solvent and heteroatom-doping source, DES cannot only significantly improve the QY of the obtained N,Cl-CDs but also extend their application fields. The obtained N,Cl-CDs demonstrated various outstanding selective fluorescence identification abilities for the Gram-positive bacteria and antibacterial ability. Thus, they could promote the possibility of overcoming Gram-positive bacterial resistance and be used as a Gram identification tool in addition to Gram staining. Compared with traditional antibacterial CDs prepared using small molecules or antibiotics−CD complexes, the N,Cl-CDs developed in this study were of green origin and had good effects on all the Gram-positive bacteria. We believe that the N,Cl-CDs may also have antibacterial effects on other bacteria, which can be further explored to develop a green and environmentally friendly bacterial identification material and antimicrobial agent. In addition, N,Cl-CDs could be used as a probe for ClO^- detection with high selectivity and sensitivity, and the biocompatibility and cell imaging capabilities of N,Cl-CDs were excellent. Therefore, the application of the prepared N,Cl-CDs is extensive, and its development may prompt other researchers to develop multifunctional CDs from other natural biomass and DESs.

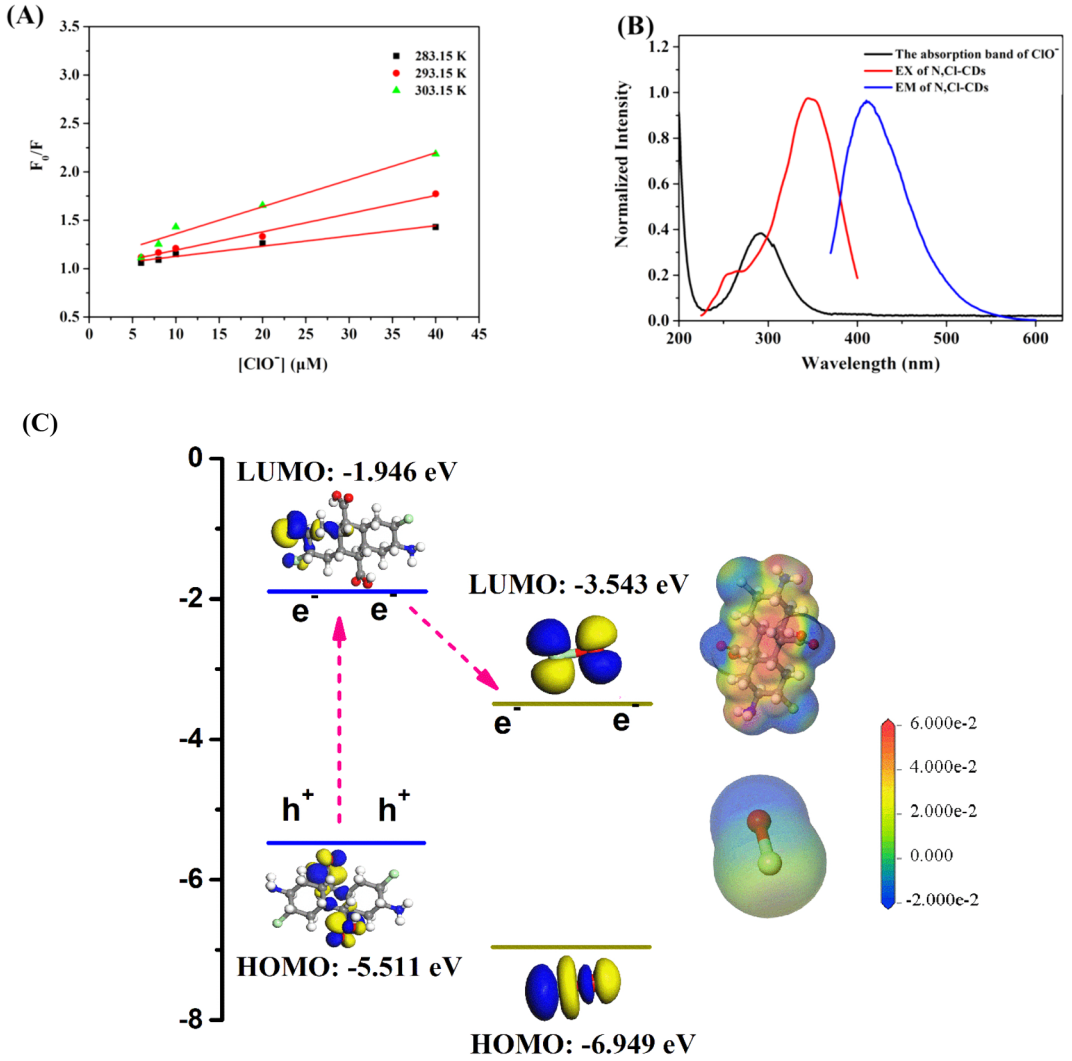

Figure 8. (A) Stern−Volmer values at different temperatures. (B) Overlap between the absorption band of ClO^- and the excitation or emission band of the N,Cl-CDs. (C) Electron transfer mechanism of N,Cl-CDs and ClO^-.

https://doi.org/10.1021/acsomega.1c04078
ACS Omega 2021, 6, 29022−29036

■ ASSOCIATED CONTENT

Supporting Information

The Supporting Information is available free of charge at https://pubs.acs.org/doi/10.1021/acsomega.1c04078.

Detailed descriptions of preparation of DESs, determination of QY of N,Cl-CDs, fluorescence emission spectra, XPS spectrum, zeta potential, and some experimental results (PDF)

■ AUTHOR INFORMATION

Corresponding Authors

Zhining Xia − *School of Pharmaceutical Sciences, Chongqing University, Chongqing 401331, China;* orcid.org/0000-0002-2064-5880; Email: tcm_anal_cqu@163.com

Xiang Li − *School of Pharmacy, Southwest Medical University, Luzhou, Sichuan 646000, China*; Email: lixiang@swmu.edu.cn

Die Gao − *School of Pharmacy, Southwest Medical University, Luzhou, Sichuan 646000, China;* orcid.org/0000-0002-2703-277X; Email: gaodie_1203@126.com

Authors

Shaochi Liu − *School of Pharmacy, Southwest Medical University, Luzhou, Sichuan 646000, China*

Tian Quan − *School of Pharmacy, Southwest Medical University, Luzhou, Sichuan 646000, China*

Lijuan Yang − *School of Pharmacy, Southwest Medical University, Luzhou, Sichuan 646000, China*

Linlin Deng − *School of Pharmacy, Southwest Medical University, Luzhou, Sichuan 646000, China*

Xun Kang − *School of Pharmacy, Southwest Medical University, Luzhou, Sichuan 646000, China*

Manjie Gao − *School of Pharmacy, Southwest Medical University, Luzhou, Sichuan 646000, China*

Complete contact information is available at: https://pubs.acs.org/10.1021/acsomega.1c04078

Notes

The authors declare no competing financial interest.

■ ACKNOWLEDGMENTS

This work was supported by the National Natural Science Foundation of China (grant no. 21904109), the Luzhou Science and Technology Bureau Innovation Miao Sub-project (no. 2019-RCM-92), a joint program of Luzhou Government and Southwest Medical University (2020LZXNYDJ25), and College Students' Innovative Entrepreneurial Training Plan Program (S20190814183X).

■ REFERENCES

(1) Dong, X.; Bond, A. E.; Pan, N.; Coleman, M.; Tang, Y.; Sun, Y.-P.; Yang, L. Synergistic Photoactivated Antimicrobial Effects of Carbon Dots Combined with Dye Photosensitizers. *Int. J. Nanomed.* **2018**, *13*, 8025−8035.

(2) Xiao, F.; Cao, B.; Wang, C.; Guo, X.; Li, M.; Xing, D.; Huo, X. Pathogen-Specific Polymeric Antimicrobials with Significant Membrane Disruption and Enhanced Photodynamic Damage To Inhibit Highly Opportunistic Bacteria. *ACS Nano* **2019**, *13*, 7356−7356.

(3) Zhu, Y.; Xu, C.; Zhang, N.; Ding, X.; Yu, B.; Xu, F.-J. Polycationic Synergistic Antibacterial Agents with Multiple Functional Components for Efficient Anti-Infective Therapy. *Adv. Funct. Mater.* **2018**, *28*, 1706709.

(4) Sun, Y.-P.; Zhou, B.; Lin, Y.; Wang, W.; Fernando, K. A. S.; Pathak, P.; Meziani, M. J.; Harruff, B. A.; Wang, X.; Wang, H. F.; Luo, P. J. G.; Yang, H.; Kose, M. E.; Chen, B. L.; Veca, L. M.; Xie, S.-Y. Quantum-Sized Carbon Dots for Bright and Colorful Photoluminescence. *J. Am. Chem. Soc.* **2006**, *128*, 7756−7757.

(5) Lv, X.; Man, H.; Dong, L.; Huang, J.; Wang, X. Preparation of Highly Crystalline Nitrogen-Doped Carbon Dots and Their Application in Sequential Fluorescent Detection of Fe^{3+} and Ascorbic Acid. *Food Chem.* **2020**, *326*, 126935.

(6) Zhao, S.; Lan, M.; Zhu, X.; Xue, H.; Ng, T.-W.; Meng, X.; Lee, C.-S.; Wang, P.; Zhang, W. Green Synthesis of Bifunctional Fluorescent Carbon Dots from Garlic for Cellular Imaging and Free Radical Scavenging. *ACS Appl. Mater. Interfaces* **2015**, *7*, 17054−17060.

(7) Ding, H.; Zhou, X. X.; Wei, J. S.; Li, X. B.; Qin, B. T.; Chen, X. B.; Xiong, H. M. Carbon Dots with Red/Near-Infrared Emissions and Their Intrinsic Merits for Biomedical Applications. *Carbon* **2020**, *167*, 322−344.

(8) Hutton, G. A. M.; Martindale, B. C. M.; Reisner, E. Carbon Dots as Photosensitisers for Solar-Driven Catalysis. *Chem. Soc. Rev.* **2017**, *46*, 6111−6123.

(9) Iravani, S.; Varma, R. S. Green Synthesis, Biomedical and Biotechnological Applications of Carbon and Graphene Quantum Dots. A Review. *Environ. Chem. Lett.* **2020**, *18*, 703−727.

(10) Rani, H.; Singh, S. P.; Yadav, T. P.; Khan, M. S.; Ansari, M. I.; Singh, A. K. *In-Vitro* Catalytic, Antimicrobial and Antioxidant Activities of Bioengineered Copper Quantum Dots Using *Mangifera indica* (L.) Leaf Extract. *Mater. Chem. Phys.* **2020**, *239*, 122052.

(11) Bhavyasree, P. G.; Xavier, T. S. Green synthesis of Copper Oxide/Carbon Nanocomposites Using the Leaf Extract of *Adhatoda vasica* Nees, Their Characterization and Antimicrobial Activity. *Heliyon* **2020**, *6*, No. e03323.

(12) Boobalan, T.; Sethupathi, M.; Sengottuvelan, N.; Kumar, P.; Balaji, P.; Gulyas, B.; Padmanabhan, P.; Selvan, S. T.; Arun, A. Mushroom-Derived Carbon Dots for Toxic Metal Ion Detection and as Antibacterial and Anticancer Agents. *Acs Appl. Nano Mater.* **2020**, *3*, 5910−5919.

(13) Shahshahanipour, M.; Rezaei, B.; Ensafi, A. A.; Etemadifar, Z. An Ancient Plant for the Synthesis of a Novel Carbon Dot and Its Applications as An Antibacterial Agent and Probe for Sensing of An Anti-cancer Drug. *Mater. Sci. Eng. C* **2019**, *98*, 826−833.

(14) Raina, S.; Thakur, A.; Sharma, A.; Pooja, D.; Minhas, A. P. Bactericidal Activity of Cannabis Sativa Phytochemicals from Leaf Extract and Their Derived Carbon Dots and Ag@Carbon Dots. *Mater. Lett.* **2020**, *262*, 127122.

(15) Yang, J.; Zhang, X.; Ma, Y.-H.; Gao, G.; Chen, X.; Jia, H.-R.; Li, Y.-H.; Chen, Z.; Wu, F.-G. Carbon Dot-Based Platform for Simultaneous Bacterial Distinguishment and Antibacterial Applications. *ACS Appl. Mater. Interfaces* **2016**, *8*, 32170−32181.

(16) Pang, Y.; Huang, Y.-K.; Li, F.; Yang, F.-Q.; Xia, Z.-N. Rapid Screening and Evaluation of Antioxidants in Alkaloid Natural Products by Capillary Electrophoresis with Chemiluminescence Detection. *Anal. Methods* **2016**, *8*, 6545−6553.

(17) Yang, J.; Gao, G.; Zhang, X.; Ma, Y.-H.; Chen, X.; Wu, F.-G. One-Step Synthesis of Carbon Dots with Bacterial Contact-Enhanced Fluorescence Emission: Fast Gram-Type Identification and Selective Gram-Positive Bacterial Inactivation. *Carbon* **2019**, *146*, 827−839.

(18) Chu, X.; Wu, F.; Sun, B.; Zhang, M.; Song, S.; Zhang, P.; Wang, Y.; Zhang, Q.; Zhou, N.; Shen, J. Genipin Cross-Linked Carbon Dots for Antimicrobial, Bioimaging and Bacterial Discrimination. *Colloids Surf., B* **2020**, *190*, 110930.

(19) Su, B. L.; Zeng, R.; Chen, J. Y.; Chen, C. Y.; Guo, J. H.; Huang, C. G. Antioxidant and Antimicrobial Properties of Various Solvent Extracts from *Impatiens balsamina L.* Stems. *J. Food Sci.* **2012**, *77*, C614−C619.

(20) Szewczyk, K.; Zidorn, C.; Biernasiuk, A.; Komsta, Ł.; Granica, S. Polyphenols from Impatiens (Balsaminaceae) and Their Antioxidant and Antimicrobial Activities. *Ind. Crops Prod.* **2016**, *86*, 262−272.

(21) Bourlinos, A. B.; Trivizas, G.; Karakassides, M. A.; Baikousi, M.; Kouloumpis, A.; Gournis, D.; Bakandritsos, A.; Hola, K.; Kozak, O.;

Zboril, R.; Papagiannouli, I.; Aloukos, P.; Couris, S. Green and Simple Route Toward Boron Doped Carbon Dots with Significantly Enhanced Non-linear Optical Properties. *Carbon* **2015**, *83*, 173−179.
(22) Marković, Z. M.; Labudová, M.; Danko, M.; Matijašević, D.; Micusik, M.; Nádaždy, V.; Kováčová, M.; Kleinová, A.; Špitalský, Z.; Pavlović, V.; Milivojević, D. D.; Medić, M.; Marković, B. M. T. Highly Efficient Antioxidant F- and Cl-Doped Carbon Quantum Dots for Bioimaging. *ACS Sustainable Chem. Eng.* **2020**, *8*, 16327−16338.
(23) Zhao, C.; Wang, X.; Wu, L.; Wu, W.; Zheng, Y.; Lin, L.; Weng, S.; Lin, X. Nitrogen-Doped Carbon Quantum Dots as An Antimicrobial Agent Against *Staphylococcus* for the Treatment of Infected Wounds. *Colloids Surf., B* **2019**, *179*, 17−27.
(24) Wang, L.; Li, Y.; Wang, Y.; Kong, W.; Lu, Q.; Liu, X.; Zhang, D.; Qu, L. Chlorine-Doped Graphene Quantum Dots with Enhanced Anti- and Pro-Oxidant Properties. *ACS Appl. Mater. Interfaces* **2019**, *11*, 21822−21829.
(25) Wu, J.; Zhang, M.; Cheng, J.; Zhang, Y.; Luo, J.; Liu, Y.; Kong, H.; Qu, H.; Zhao, Y. Effect of *Lonicerae japonicae* Flos Carbonisata-Derived Carbon Dots on Rat Models of Fever and Hypothermia Induced by Lipopolysaccharide. *Int. J. Nanomed.* **2020**, *15*, 4139−4149.
(26) Li, L.; Wang, X.; Fu, Z.; Cui, F. One-Step Hydrothermal Synthesis of Nitrogen- and Sulfur-co-Doped Carbon Dots from Ginkgo Leaves and Application in Biology. *Mater. Lett.* **2017**, *196*, 300−303.
(27) Zhang, Q.; Vigier, K. D. O.; Royer, S.; Jérôme, F. Deep Eutectic Solvents: Syntheses, Properties and Applications. *Chem. Soc. Rev.* **2012**, *41*, 7108−7146.
(28) Wang, X.; Cheng, Z.; Zhou, Y.; Tammina, S. K.; Yang, Y. A Double Carbon Dot System Composed of N, Cl-Doped Carbon Dots and N, Cu-Doped Carbon Dots as Peroxidase Mimics and as Fluorescent Probes for the Determination of Hydroquinone by Fluorescence. *Microchim. Acta* **2020**, *187*, 350.
(29) Wang, N.; Zheng, A.-Q.; Liu, X.; Chen, J.-J.; Yang, T.; Chen, M.; Wang, J.-H. Deep Eutectic Solvent-Assisted Preparation of Nitrogen/Chloride-Doped Carbon Dots for Intracellular Biological Sensing and Live Cell Imaging. *ACS Appl. Mater. Interfaces* **2018**, *10*, 7901−7909.
(30) Wang, M.; Kang, X.; Deng, L.; Wang, M.; Xia, Z.; Gao, D. Deep Eutectic Solvent Assisted Synthesis of Carbon Dots Using Sophora Flavescens Aiton Modified with Polyethyleneimine: Application in Myricetin Sensing and cell Imaging. *Food Chem.* **2021**, *345*, 128817−128817.
(31) Wan, Y.; Wang, M.; Zhang, K.; Fu, Q.; Wang, L.; Gao, M.; Xia, Z.; Gao, D. Extraction and Determination of Bioactive Flavonoids from *Abelmoschus manihot* (Linn.) Medicus Flowers Using Deep Eutectic Solvents Coupled with High-Performance Liquid Chromatography. *J. Sep. Sci.* **2019**, *42*, 2044−2052.
(32) 46th ESAO Congress 3-7 September 2019 Hannover, Germany Abstracts. *Int. J. Artif. Organs* **2019**, *42* (), 386−474, DOI: 10.1177/0391398819860985.
(33) Atchudan, R.; Edison, T. N. J. I.; Perumal, S.; Muthuchamy, N.; Lee, Y. R. Hydrophilic Nitrogen-Doped Carbon Dots from Biowaste Using Dwarf Banana Peel for Environmental and Biological Applications. *Fuel* **2020**, *275*, 117821.
(34) Jang, S. J.; Kang, Y. C.; Roh, K. C. Preparation of Activated Carbon Decorated with Carbon Dots and Its Electrochemical Performance. *J. Ind. Eng. Chem.* **2020**, *82*, 383−389.
(35) Cheng, H.; Bian, Y.; Wang, F.; Jiang, X.; Ji, R.; Gu, C.; Yang, X.; Song, Y. Green Conversion of Crop Residues into Porous Carbons and Their Application to Efficiently Remove Polycyclic Aromatic Hydrocarbons from Water: Sorption Kinetics, Isotherms and Mechanism. *Bioresour. Technol.* **2019**, *284*, 1−8.
(36) Yang, X.; Xu, J.; Luo, N.; Tang, F.; Zhang, M.; Zhao, B. N,Cl co-Doped Fluorescent Carbon Dots as Nanoprobe for Detection of Tartrazine in Beverages. *Food Chem.* **2020**, *310*, 125832.
(37) Zhu, J.; Chu, H.; Wang, T.; Wang, C.; Wei, Y. Fluorescent Probe Based Nitrogen Doped Carbon Quantum Dots with Solid-State Fluorescence for the Detection of Hg^{2+} and Fe^{3+} in Aqueous Solution. *Microchem. J.* **2020**, *158*, 105142.
(38) Wang, C.; Shi, H.; Yang, M.; Yan, Y.; Liu, E.; Ji, Z.; Fan, J. Facile Synthesis of Novel Carbon Quantum Dots from Biomass Waste for Highly Sensitive Detection of Iron Ions. *Mater. Res. Bull.* **2020**, *124*, 110730.
(39) He, W.; Huo, Z.; Sun, X.; Shen, J. Facile and Green Synthesis of N, Cl-Dual-Doped Carbon Dots as A Label-Free Fluorescent Probe for Hematin and Temperature Sensing. *Microchem. J.* **2020**, *153*, 104528.
(40) Wang, R.; Wang, R.; Ju, D.; Lu, W.; Jiang, C.; Shan, X.; Chen, Q.; Sun, G. ″On-Off-On″ Fluorescent Probes Based on Nitrogen-Doped Carbon Dots for Hypochlorite and Bisulfite Detection in Living Cells. *Analyst* **2018**, *143*, 5834−5840.
(41) Wei, Z.; Li, H.; Liu, S.; Wang, W.; Chen, H.; Xiao, L.; Ren, C.; Chen, X. Carbon Dots as Fluorescent/Colorimetric Probes for Real-Time Detection of Hypochlorite and Ascorbic Acid in Cells and Body Fluid. *Anal. Chem.* **2019**, *91*, 15477−15483.
(42) Liu, J.; Lu, S.; Tang, Q.; Zhang, K.; Yu, W.; Sun, H.; Yang, B. One-Step Hydrothermal Synthesis of Photoluminescent Carbon Nanodots with Selective Antibacterial Activity Against *Porphyromonas gingivalis*. *Nanoscale* **2017**, *9*, 7135−7142.
(43) Wang, H.; Zhang, L.; Guo, X.; Dong, W.; Wang, R.; Shuang, S.; Gong, X.; Dong, C. Comparative Study of Cl,N-Cdots and N-Cdots and Application for Trinitrophenol and ClO^- Sensor and Cell-Imaging. *Anal. Chim. Acta* **2019**, *1091*, 76−87.
(44) Ruiz, V.; Yate, L.; Garcia, I.; Cabanero, G.; Grande, H.-J. Tuning the Aantioxidant Activity of Graphene Quantum Dots: Protective Nanomaterials Against Dye Decoloration. *Carbon* **2017**, *116*, 366−374.
(45) Wang, M.; Wan, Y.; Zhang, K.; Fu, Q.; Wang, L.; Zeng, J.; Xia, Z.; Gao, D. Green Synthesis of Carbon Dots Using the Flowers of *Osmanthus Fragrans* (Thunb.) Lour. as Precursors: Application in Fe^{3+} and Ascorbic Acid Determination and Cell Imaging. *Anal. Bioanal. Chem.* **2019**, *411*, 2715−2727.
(46) Huang, X.; Li, Y.; Zhong, X.; Rider, A. E.; Ostrikov, K. K. Fast Microplasma Synthesis of Blue Luminescent Carbon Quantum Dots at Ambient Conditions. *Plasma Processes Polym.* **2015**, *12*, 59−65.
(47) Isnaeni; Zufara, B. S.; Lewa, I. W. L.; Herbani, Y.; Shiddiq, M. Role of Surface States on Luminescence Shift of Caramelised Sugar Carbon Dots for Color Conversion Emitting Devices. *Adv. Nat. Sci. Nanosci.* **2020**, *11*, No. 015003.
(48) Cremin, K.; Jones, B. A.; Teahan, J.; Meloni, G. N.; Perry, D.; Zerfass, C.; Asally, M.; Soyer, O. S.; Unwin, P. R. Scanning Ion Conductance Microscopy Reveals Differences in the Ionic Environments of Gram-Positive and Negative Bacteria. *Anal. Chem.* **2020**, *92*, 16024−16032.
(49) Gagic, M.; Kociova, S.; Smerkova, K.; Michalkova, H.; Setka, M.; Svec, P.; Pribyl, J.; Masilko, J.; Balkova, R.; Heger, Z.; Richtera, L.; Adam, V.; Milosavljevic, V. One-Pot Synthesis of Natural Amine-Modified Biocompatible Carbon Quantum Dots with Antibacterial Activity. *J. Colloid Interface Sci.* **2020**, *580*, 30−48.
(50) Abu Rabe, D. I.; Al Awak, M. M.; Yang, F.; Okonjo, P. A.; Dong, X.; Teisl, L. R.; Wang, P.; Tang, Y.; Pan, N.; Sun, Y. P.; Yang, L. The Ddominant Role of Surface Functionalization in Carbon Dots' Photo-Activated Antibacterial Activity. *Int. J. Nanomed.* **2019**, *14*, 2655−2665.
(51) Han, J.; Cheng, H.; Wang, B.; Braun, M. S.; Fan, X.; Bender, M.; Huang, W.; Domhan, C.; Mier, W.; Lindner, T.; Seehafer, K.; Wink, M.; Bunz, U. H. F. A Polymer/Peptide Complex-Based Sensor Array That Discriminates Bacteria in Urine. *Angew. Chem., Int. Ed.* **2017**, *56*, 15246−15251.
(52) Uzarski, J. R.; Mello, C. M. Detection and Classification of Related Lipopolysaccharides via a Small Array of Immobilized Antimicrobial Peptides. *Anal. Chem.* **2012**, *84*, 7359−7366.
(53) Jian, H. J.; Wu, R. S.; Lin, T. Y.; Li, Y. J.; Lin, H. J.; Harroun, S. G.; Lai, J. Y.; Huang, C. C. Super-Cationic Carbon Quantum Dots Synthesized from Spermidine as an Eye Drop Formulation for Topical Treatment of Bacterial Keratitis. *ACS Nano* **2017**, *11*, 6703−6716.
(54) Bing, W.; Sun, H.; Yan, Z.; Ren, J.; Qu, X. Programmed Bacteria Death Induced by Carbon Dots with Different Surface Charge. *Small* **2016**, *12*, 4713−4718.
(55) Dwyer, D. J.; Belenky, P. A.; Yang, J. H.; MacDonald, I. C.; Martell, J. D.; Takahashi, N.; Chan, C. T. Y.; Lobritz, M. A.; Braff, D.; Schwarz, E. G.; Ye, J. D.; Pati, M.; Vercruysse, M.; Ralifo, P. S.; Allison, K. R.; Khalil, A. S.; Ting, A. Y.; Walker, G. C.; Collins, J. J. Antibiotics

https://doi.org/10.1021/acsomega.1c04078
ACS Omega 2021, 6, 29022−29036

induce redox-related physiological alterations as part of their lethality. *Proc. Natl. Acad. Sci. U. S. A.* **2014**, *111*, E2100−E2109.
(56) Zu, F.; Yan, F.; Bai, Z.; Xu, J.; Wang, Y.; Huang, Y.; Zhou, X. The Quenching of the Fluorescence of Carbon Dots: A Review on Mechanisms and Applications. *Microchim. Acta* **2017**, *184*, 1899−1914.
(57) Hou, J.; Tian, Z.; Xie, H.; Tian, Q.; Ai, S. A Fluorescence Resonance Energy Transfer Sensor Based on Quaternized Carbon Dots and Ellman's Test for Ultrasensitive Detection of Dichlorvos. *Sens. Actuators, B* **2016**, *232*, 477−483.
(58) Roy, S.; Bardhan, S.; Mondal, D.; Saha, I.; Roy, J.; Das, S.; Chanda, D. K.; Karmakar, P.; Das, S. Polymeric Carbon Dot/Boehmite Nanocomposite Made Portable Sensing Device (Kavach) for Non-Invasive and Selective Detection of Cr(VI) in Wastewater and Living Cells. *Sens. Actuators, B* **2021**, *348*, 130662.

https://doi.org/10.1021/acsomega.1c04078
ACS Omega 2021, 6, 29022−29036